

Oscillating plasma bubbles. II. Pulsed experiments

R. L. Stenzel and J. M. Urrutia

Department of Physics and Astronomy, University of California, Los Angeles, California 90095-1547, USA

(Received 17 April 2012; accepted 7 June 2012; published online 6 August 2012)

Time-dependent phenomena have been investigated in plasma bubbles which are created by inserting spherical grids into an ambient plasma and letting electrons and ions form a plasma of different parameters than the ambient one. There are no plasma sources inside the bubble. The grid bias controls the particle flux. There are sheaths on both sides of the grid, each of which passes particle flows in both directions. The inner sheath or plasma potential develops self consistently to establish charge neutrality and divergence free charge and mass flows. When the electron supply is restricted, the inner sheath exhibits oscillations near the ion plasma frequency. When all electrons are excluded, a virtual anode forms on the inside sheath, reflects all ions such that the bubble is empty. By pulsing the ambient plasma, the lifetime of the bubble plasma has been measured. In an afterglow, plasma electrons are trapped inside the bubble and the bubble decays as slow as the ambient plasma. Pulsing the grid voltage yields the time scale for filling and emptying the bubble. Probes have been shown to modify the plasma potential. Using pulsed probes, transient ringing on the time scale of ion transit times through the bubble has been observed. The start of sheath oscillations has been investigated. The instability mechanism has been qualitatively explained. The dependence of the oscillation frequency on electrons in the sheath has been clarified. © 2012 American Institute of Physics. [<http://dx.doi.org/10.1063/1.4743020>]

I. INTRODUCTION

Since sheaths are ubiquitous in plasma physics their stability is a topic of broad interest. Many observations of sheath instabilities have been reported. Electron-rich sheaths can oscillate at the electron plasma frequency.^{1,2} Ion-rich sheaths with restricted electron supply can oscillate near the ion plasma frequency.^{3–7} Virtual cathodes and anodes are special cases of sheaths which are highly unstable.^{8,9} Electron-rich sheaths in magnetized plasmas can destabilize electron drift waves.¹⁰ In the presence of neutrals, electron-rich sheaths can produce ionization instabilities¹¹ which can expand into pulsating discharge phenomena with ionization double layers.^{12–17}

In the present work, the properties of an enclosed plasma within an ambient plasma have been investigated. The two plasmas are separated by a highly transparent grid which is biased negatively. The grid bias forms two ion rich sheaths which carry ion and electron flows in both directions. The inner plasma, termed a “bubble,” has no plasma source and is formed by electron and ion inflows. In steady state, the flows must be divergence free which is established self-consistently by the plasma potential or sheath of the bubble. The steady-state properties of the bubble and the sheath instability have been described in a companion paper.¹⁸ The present paper describes time resolved measurements for pulsed plasmas, pulsed grid voltages, and pulsed probes. These reveal the time scale for filling and emptying of the bubble, the trapping of electrons, the probe perturbations on trapped electrons, and transient sheath ringing and the onset of the sheath instability near the ion plasma frequency. In particular, the role of electrons in an ion rich sheath in determining the frequency of the instability has been explained. Sheath oscillations arise from the inertia of the ions which

causes them to move in the direction opposite to the space charge field they created. The ion space charge perturbations cannot be neutralized by electrons when the electron flux is restricted to be equal to the ion flux. In the limit of no electron supply, the sheath becomes a virtual anode which oscillated at the ion plasma frequency of the ambient plasma.

Neutralizing electrons can either be supplied from the ambient plasma or by an electron source inserted into the bubble. The latter case will be described in a third companion paper.¹⁹ The present paper is organized as follows: After briefly describing the experimental setup and pulse circuits in Sec. II, the observations of time-resolved bubble properties, sheath transients and instabilities will be presented in Sec. III. The findings are summarized in the Conclusion.

II. EXPERIMENTAL ARRANGEMENT

A low temperature discharge plasma of typical density $n_e \simeq 10^9 \text{ cm}^{-3}$, electron temperature $kT_e \simeq 2 \text{ eV}$, has been produced by a dc discharge in Argon at a pressure $p \simeq 3 \times 10^{-4} \text{ mTorr}$ in a chamber of dimensions 45 cm in diameter and 100 cm length as described in a companion paper.¹⁸

Since the present paper mainly describes pulsed plasma bubbles, Fig. 1 shows a schematic sketch of the typical pulsing circuit. A gridded sphere of typically 8 cm diam made of fine mesh wire (mesh size 0.25 mm, 80% transparency) is inserted into the ambient plasma. The grid is biased negatively which attracts ions into the sphere but limits the electron influx to tail electrons with energy $mv_{perp}^2/2 > e|V_{grid}|$. The bubble plasma is formed by injection of ions and electrons rather than by ionization. The plasma parameters are measured with a radially movable Langmuir probe. An emissive probe in the center of the bubble is used to measure the

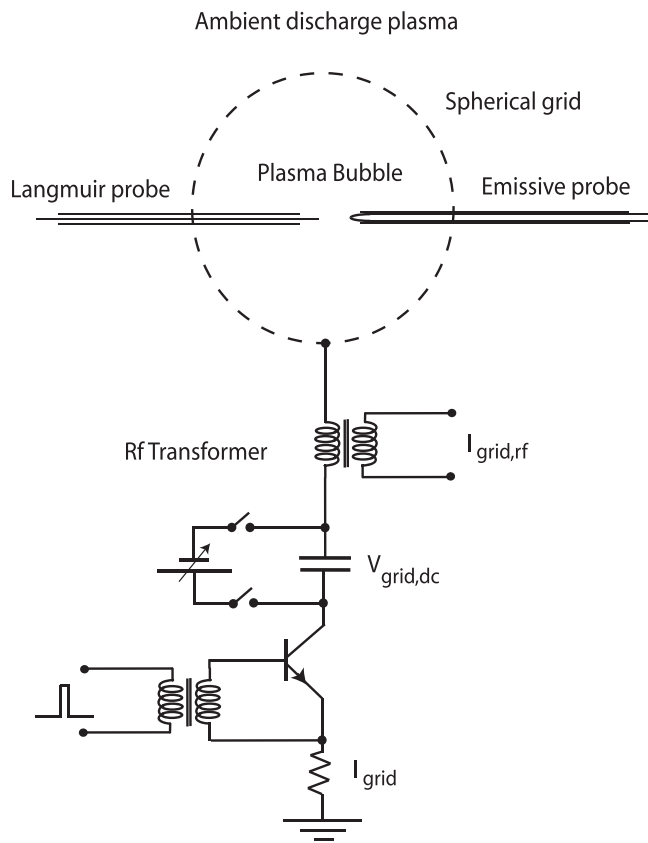


FIG. 1. Schematic setup to produce and diagnose pulsed plasma bubbles in an ambient discharge plasma.

approximate plasma potential and to inject electrons into the bubble to neutralize the ion space charge. The probe diagnostics requires careful interpretation since the probe currents can modify the plasma properties, as will be shown below. Even the ceramic probe shaft presents a perturbation since it causes surface recombination of confined charged particles.

The grid voltage is pulsed with the switching circuit shown in Fig. 1. In order to minimize capacitances to ground the power supply consists of a charged, floating capacitor ($4000 \mu\text{F}$, 250 V). The switching circuit consists of a simple transistor switch. The grid current is obtained from the voltage drop of a series resistor to ground. Grid current oscillations are measured with a rf broadband transformer (100 kHz–100 MHz) inserted close to the grid feed which minimizes stray capacitive currents.

The same switching circuit has also been used to pulse the ambient discharge plasma. Likewise, pulsed voltages have been applied to the Langmuir probe and the emissive probe. The emissive probe requires a heater power supply which has a large capacitance to ground. In order to prevent capacitive currents, the emissive probe (0.125 mm diam, 5 mm length W wire) is heated with a floating battery (3 V, 2 A). For measuring floating potentials, a 10:1 oscilloscope probe (20 pF, 10 M Ω) is used or a capacitive divider with a low voltage high impedance ($10^{15} \Omega$) op amp.

All signals are acquired with a 4-channel digital oscilloscope with bandwidth up to 400 MHz and up to 2.5×10^6 samples stored.

III. EXPERIMENTAL RESULTS

Before describing the time-resolved measurements, it is useful to summarize the basic dc properties of plasma bubbles. Bubbles are here defined as plasma volumes separated from an ambient plasma by a biased grid. A positive bias leads to discharge phenomena and transit time instabilities which have been studied earlier.²⁰ In the present experiments, the grid is biased negatively. Ions are accelerated toward the grid, partly collected on the wire, but mainly injected through the mesh openings into the bubble. The ion flux is given by the Bohm current which for a plane sheath is nearly independent of the grid bias. The electron current, however, strongly depends on the grid voltage, $I \propto \exp(eV_{grid}/kT_e)$ for a Maxwellian distribution. In a dc discharge, there is a tail of energetic electrons with peak energy given by the discharge or cathode voltage. When the grid voltage exceeds the discharge voltage, all electrons are repelled. The injected ions build up a space charge layer ("virtual anode") which also repels them such that the bubble is void of plasma.

In steady state, the bubble plasma has to satisfy two conditions: The net current and net mass flow into the bubble must be divergence free. This is obvious for any uniform plasma volume without a bounding sheath. In the absence of electrodes inside the bubble, there would be no closure for currents into the bubble which therefore must vanish. Likewise, the mass flow must be zero in the absence of particle sources and sinks in order to have a constant density in steady-state. In addition, the electron and ion densities have to be equal in a dense bubble plasma. These requirements have to be established self-consistently by the sheath or plasma potential inside the bubble. Deviations from these requirements can lead to unstable sheaths which are observed as oscillations near the ion plasma frequency.

The grid has two sheaths, one facing the ambient plasma, the other facing the bubble. The outer sheath has been found to be stable while the inner one oscillates when the electron inflow is limited to the ion inflow. The sheath potential drops are in general different. The double sheaths differ from single sheaths on solid boundaries because they carry flows in both directions. For a given ion inflow, the inner sheath must adjust such that the ion outflow balances the inflow minus losses on the grid. For example, when all electrons are reflected, the plasma potential inside the bubble rises above the ambient plasma potential to reflect all ions.

Likewise, the electrons entering the bubble must leave minus those lost on the grid wire or by surface recombination. Since both the injected electron and ion densities are small compared to the observed bubble density, the particles do not just stream freely through the bubble but must be partially trapped or confined. This arises from scattering at the sheaths. Particles acquire or lose energy when entering the bubble but they cannot exit the bubble on the opposite side unless they are incident normal to the sheath. Most particles are oblique to the sheath since the grid does not have a precise spherical shape and the grid wires produce non-radial field components. Trapping by multiple reflections raises the density. The filling and emptying of the bubble will demonstrate the confinement of particles.

Although no direct evidence for ion beam-plasma instabilities has been observed, the injected ions could also be scattered by micro turbulence inside the bubble. The resultant loss of momentum or energy would trap the injected ions.

The steady state properties of bubble plasmas have been established in the first companion paper.¹⁸ Now, we show how the steady state is reached when the grid voltage or ambient density or probe perturbations are switched on and off. Useful information about the instability is obtained by triggering it and observing amplitude growth and frequency changes.

A. Pulsed discharges

In order to vary the electron distributions of the ambient plasma, the discharge has been pulsed. During the active discharge, the electrons have two populations: Primary electrons with energy given by the discharge voltage (20–80 V) plus the voltage drop along the cathode filament ($\simeq 7$ V) and the bulk of secondary low temperature (2 eV) electrons created by ionization. In the afterglow, the primaries are absent and the secondaries have a Maxwellian distribution.

Probes are usually used to measure the energy distribution, but in a bubble plasma the restricted electron supply is easily perturbed by a probe as shown in Fig. 2. The probe is biased to a fixed voltage and the current is recorded vs time during the discharge and afterglow. From a family of current-voltage (I–V) traces shown in Fig. 2(a), the probe characteristics can be constructed at different times as shown

in Fig. 2(b). At the start of the discharge (t_1, t_2), a relatively large population of energetic electrons is present which passes through the grid biased at the discharge voltage. The ion current rises as the ambient plasma is produced. In the afterglow, no cold electrons can enter or leave the bubble. When the probe is biased negatively, the ion current decays slowly but when it is biased positively the current decays faster and as more electrons are collected the decay rate increases. The reason is that the probe depletes the electrons trapped inside the bubble. When I–V traces are constructed in the afterglow they exhibit a negative slope. The electron current decreases with probe voltage since the electrons are depleted faster at high probe currents. Similar depletion effects have been studied earlier.²¹

The probe current affects the sheath oscillations as shown in Fig. 2(c). As the density rises, the sheath oscillations start and continue well into the afterglow due to electron and ion trapping. However, when the probe depletes the electrons ($V_{probe} > 0$) the instability approaches the virtual anode oscillation which has a smaller amplitude, higher frequency, and shorter duration in the afterglow. Figure 2(d) displays the spectrum of the oscillations in the afterglow during a time interval indicated in Fig. 2(c). Since the density decays, the line width is broadened but the upshift in frequency upon electron depletion by the probe is clearly visible.

Since the bubble plasma is starved for electrons, it is easily perturbed by both electron collection and emission. The collection of ions produces little perturbations since the ion flow through the negatively biased grid is not restricted.

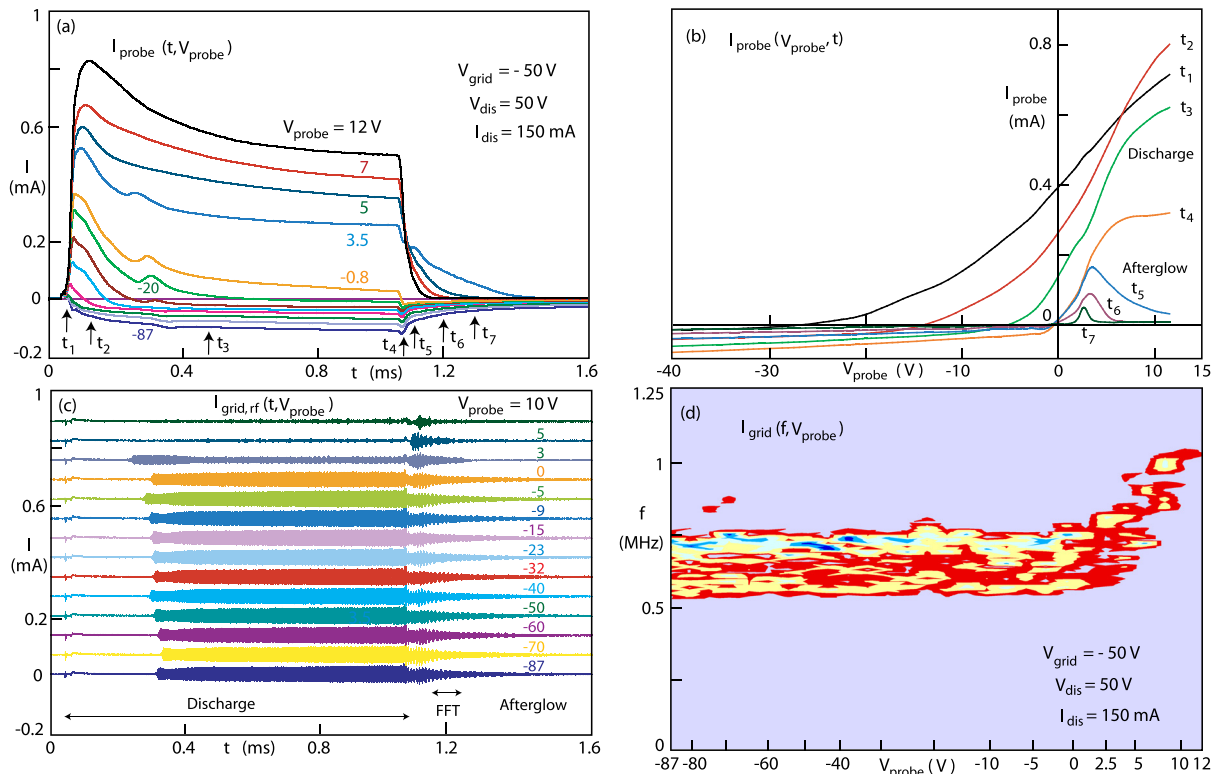


FIG. 2. Probe I–V curve inside a plasma bubble embedded in a pulsed discharge plasma. (a) Probe current vs time for different probe voltages, showing a voltage-dependent electron decay time shorter than the ion decay. It is caused by electron depletion by the probe which (b) results in probe I–V curves with a negative differential conductance, $dI/dV < 0$, in the afterglow where no electrons can enter the sphere. (c) Rf waveform of the grid current for different probe voltages. Note oscillations extend into the afterglow where electrons are trapped inside the bubble. (d) Spectrum of the oscillations in the afterglow [time indicated in (c)] as a function of probe voltage. The line is broad since the density decays during the FFT. When the probe collects electrons the frequency rises.

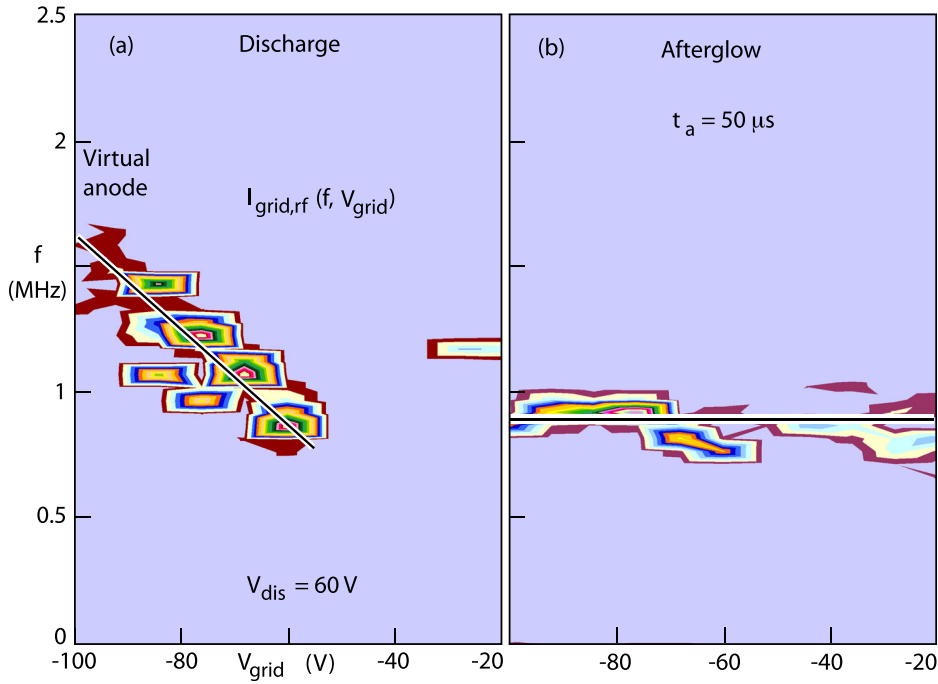


FIG. 3. Spectra of $I_{grid,rf}$ vs V_{grid} (a) during the discharge and (b) in the afterglow. The frequency increases with negative grid bias which reduces the inflow of electrons into the bubble. In the afterglow, the frequency $f(V_{grid})$ remains nearly constant since the grid does not allow low energy electrons to either enter or leave the sphere. Electrons are trapped inside the bubble, while ions pass through the grid. The bubble plasma decays at the same rate as the ambient plasma.

The trapping of electrons in the afterglow can also be demonstrated by comparing the frequency dependence on grid voltage in the discharge and afterglow, presented in Fig. 3. In the discharge, the electron flux into the bubble is reduced when the grid is biased more negatively. This leads to an increase in the frequency of the instability as shown in Fig. 3(a). For low V_{grid} , the electron supply is abundant which usually results in stable sheaths. Figure 3(b) shows that in the afterglow the frequency does not depend on V_{grid} because low energy electrons cannot pass through the grid, hence the electron flow does not change with V_{grid} . Electrons must be trapped in the bubble since the frequency is much lower than that of virtual anode oscillations.

How long electrons are trapped is demonstrated in Fig. 4. Although decaying, the oscillations in $I_{grid,rf}$ are observable for at least 300 μs [Fig. 4(a)]. By measuring the rf period at discrete intervals, one obtains a plot of $f(t)$ [Fig. 4(b)]. Since the frequency scales proportional to the plasma frequency a plot of f^2 is proportional to the density decay, conveniently displayed on a logarithmic scale. The e-folding density decay inside the bubble has a time constant $\tau \approx 100 \mu s$ which is comparable to that of the outside plasma measured from the ion current to the grid [Fig. 4(c)]. Thus, the bubble plasma decays at the same rate as the ambient plasma. Electrons which entered during the discharge are confined inside the bubble. Ions can pass the grid and equalize the inside and outside densities.

B. Pulsed grid voltage

The grid voltage controls the electron flow into the bubble. For large negative voltages, the electrons cannot enter the sphere and a large positive space charge layer develops near the inner grid which reflects the incident ions, leaving the volume essentially empty. By pulsing the grid voltage, the growth and decay of the bubble can be observed.

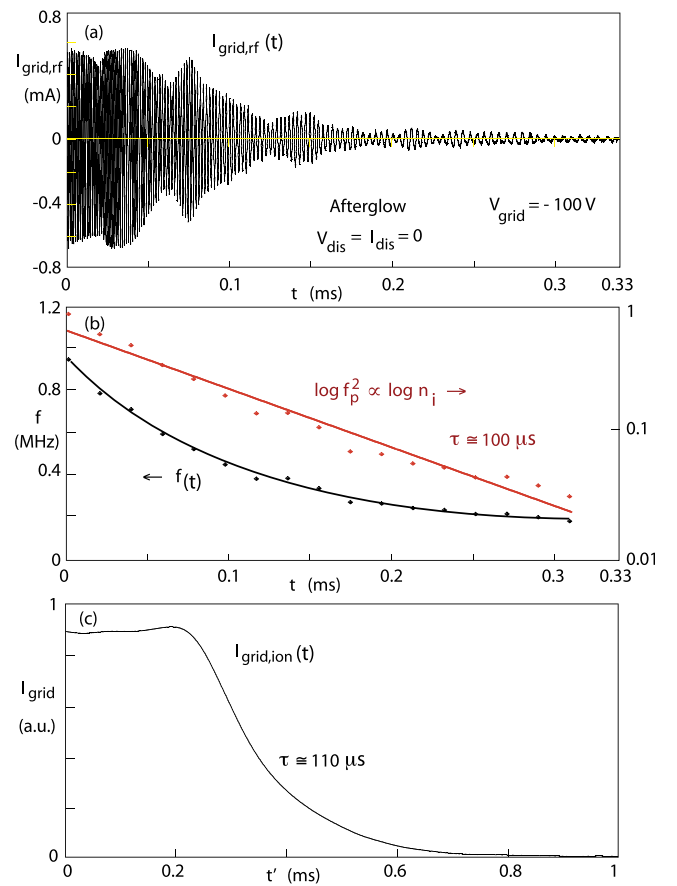


FIG. 4. Sheath instability in an afterglow plasma. (a) Oscillations in the grid current of a biased sphere whose frequency decays in time. (b) Frequency decay vs time, $f(t)$. Since the frequency is proportional to the plasma frequency, a plot of $\log f_p^2$ yields the density decay time *inside* the oscillating bubble. (c) The density decay of the *outside* plasma, obtained from the decaying ion grid current, is comparable to the bubble decay. Electrons are trapped in the bubble while ions flow in and out of the bubble.

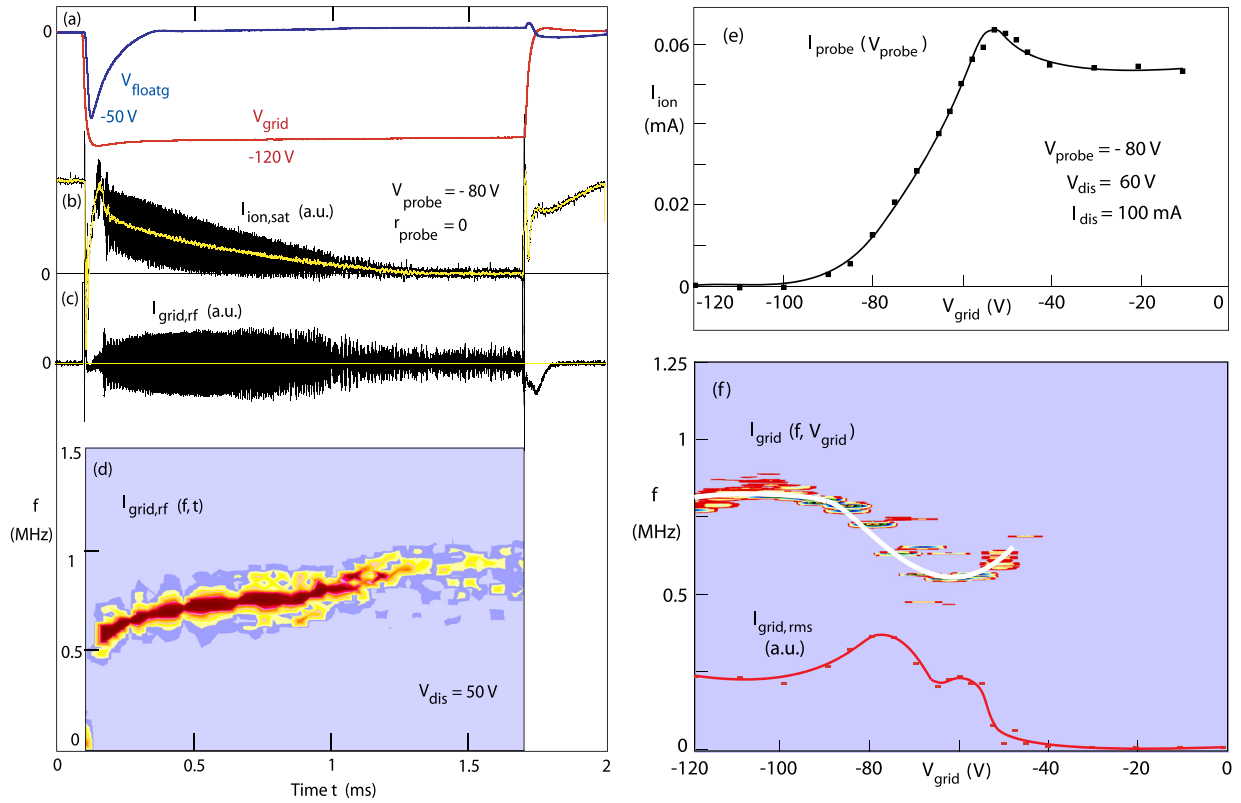


FIG. 5. Pulsed grid voltage to observe the emptying and filling of a plasma bubble. (a) Grid voltage $V_{\text{grid}}(t)$ and the floating potential measured with a second probe near the center of the sphere. Initially, the floating potential approaches the discharge voltage, indicating trapping of primary electrons. (b) Ion saturation current to a Langmuir probe in the center of the 8 cm diam sphere (instantaneous and mean values). The ions are expelled slowly because the electrons are trapped and both species must decay at the same rate. (c) Oscillations in the grid current which continue as virtual anode oscillations when the bubble is empty. (d) Time-resolved spectrum of the grid current oscillations showing a frequency rise while the density in the bubble decreases. Thus, the ion plasma frequency in the vicinity of the grid rather than in the bubble volume determines the instability frequency. (e) Dc ion current vs grid voltage in a dc discharge showing an empty bubble at large negative grid voltages. (f) Frequency and amplitude dependence of $I_{\text{grid},\text{rf}}$ vs $V_{\text{grid},dc}$.

Figure 5 summarizes the main observations of emptying and refilling of the bubble. In a dc discharge, the grid voltage is pulsed from 0 to $V_{\text{grid}} = -120$ V which stops primary electrons of energy $eV_{\text{dis}} = 50$ eV from either entering or leaving the bubble. Due to the electron trapping, a large negative transient floating potential develops [Fig. 5(a)]. The ions cannot leave the bubble while the electrons are trapped [Fig. 5(b)]. The decay is *not* given by the ion transit time through the bubble but by the electron loss. Surface recombination on the ceramic probe shafts is the major loss since neither grid nor probe collects electrons.

One can estimate the electron decay as follows: The probe shaft is 2 mm in diameter and 4 cm long when the probe is in the center of the sphere. The probe surface area is $2\pi r_{\text{probe}} l_{\text{probe}} \simeq 2.5$ cm². The electron flux to a nonconducting surface equals the ion flux, $I_e = I_i = A_{\text{probe}} n e v_i$. The electron current leads to a decay of the electron charge inside the bubble, $I_e = (dn/dt)e(4/3)\pi r_{\text{bubble}}^3$. Thus, for $v_i \simeq 2 \times 10^5$ cm/s and $r_{\text{bubble}} = 4$ cm, the decay time constant is $\tau = n/(dn/dt) = (4/3)\pi r_{\text{bubble}}^3 / (A_{\text{probe}} v_i) \simeq 0.54$ ms, which agrees with the observed decay time $I_{\text{ion}}/(dI_{\text{ion}}/dt) \simeq 0.5$ ms in Fig. 5(b).

The impact of 120 eV ions on the stainless steel grid does not release sufficient secondary electrons to balance the electron losses. After about 1 ms, there are no ions or electrons left in the center of the bubble.

The instability is visible on the probe as long as there is plasma in the center of the bubble. On the grid, the oscillations continue while the bubble is empty, showing again that the instability arises from the sheath [Fig. 5(c)]. By dividing the waveform into 50 bins, 400 samples each, and performing a fast Fourier transform (FFT) of each, a time-resolved spectrum of $I_{\text{grid},\text{rf}}$ is obtained [Fig. 5(d)]. As electrons are gradually removed from the sheath, the frequency increases to that of virtual anode oscillations.

When the grid voltage is turned off, the empty bubble refills [$t > 1.7$ ms, Fig. 5(b)]. Analogous to free plasma expansion into vacuum electrons and ions expand together at the ion transit time into the sphere. The abundant electron supply from the ambient plasma prevents the sheath from oscillating. When the electron supply is limited, e.g., by switching the grid voltage to V_{dis} instead of 0, the ion flux rises slowly and linearly in time at a rate controlled by the electron flux (not shown).

The amplitude of the grid voltage pulse has been varied in a steady-state plasma. As shown in Fig. 5(e), the ion current in the bubble vanishes only when the grid voltage is more negative than the discharge voltage. For smaller grid voltages, the ion influx is not inhibited by the grid voltage. A small enhancement in the ion flux is observed when the grid begins to stagnate the primary electrons.

The spectrum and amplitude of the instability in the grid current as a function of grid voltage are shown in Fig. 5(f).

When the bubble is empty ($V_{grid} = -100$ V) the frequency of the virtual anode oscillations has a maximum. Leaking electrons into the bubble lowers the frequency and increases the oscillation amplitude. The frequency minimum occurs for $|V_{grid}| \simeq V_{dis}$ where electrons stagnate in the sheath. For small grid voltages, the increase in electron supply prevents the sheath instability.

C. Pulsed probes

Since there is no electron sink, i.e., an anode, inside the bubble, the plasma potential is not specified and can be easily perturbed, particularly by electron-collecting probes. In order to minimize the probe current, a small cylindrical Langmuir probe is used (0.125 mm Ta, 3 mm long) for the diagnostics. The I-V characteristics exhibit no features to identify the plasma potential which is the result of changing the plasma potential by the probe bias. Although the plasma potential cannot be obtained correctly at least the floating potential can be measured reliably since $I_{probe} = 0$ produces the least perturbation. A second probe, the cold emissive probe in the center of the sphere is biased while the Langmuir probe measures the floating potential near the sheath ($r_{probe} \simeq 4$ cm). The bias is pulsed so as to observe the time evolution of the potential change.

Figure 6 summarizes the effects of pulsing the center probe. Both a positive and a negative pulse affect the floating

potential, hence also the plasma potential [Fig. 6(a)]. The perturbation depends on grid voltage and is largest where the floating potential assumes a minimum [Fig. 6(b)]. The fact that both polarities cause potential perturbations indicates that the plasma potential is not only determined by electrons but also by ion losses. This is also evident from the long time scale for potential changes which is not determined by particle transit times through the sheath or sphere but is characteristic for the particle trapping time. The time scale for the potential adjustment after the end of the probe pulse increases with $|V_{grid}|$ due to the restricted electron inflow. When the probe is biased to +15 V, it is well above the plasma potential, hence draws electron saturation current. The current must be closed through the grid to ground. Since the influx of ions and electrons is determined by the constant grid potential, the outflow of particles from the bubble must be changed. This is accomplished by the rising plasma potential which increases the potential drop across the sheath and reduces the electron outflow. The probe collects some of the trapped electrons which lowers the electron density and modifies the instability.

Figure 6(c) shows how the positive probe pulse affects the sheath instability. The negative pulse does not modify the instability, hence is not shown. Prior to the positive pulse, the instability does not exist for low V_{grid} where the inflow of electrons is high. The positive probe pulse extracts electrons which triggers sheath oscillations at lower V_{grid}

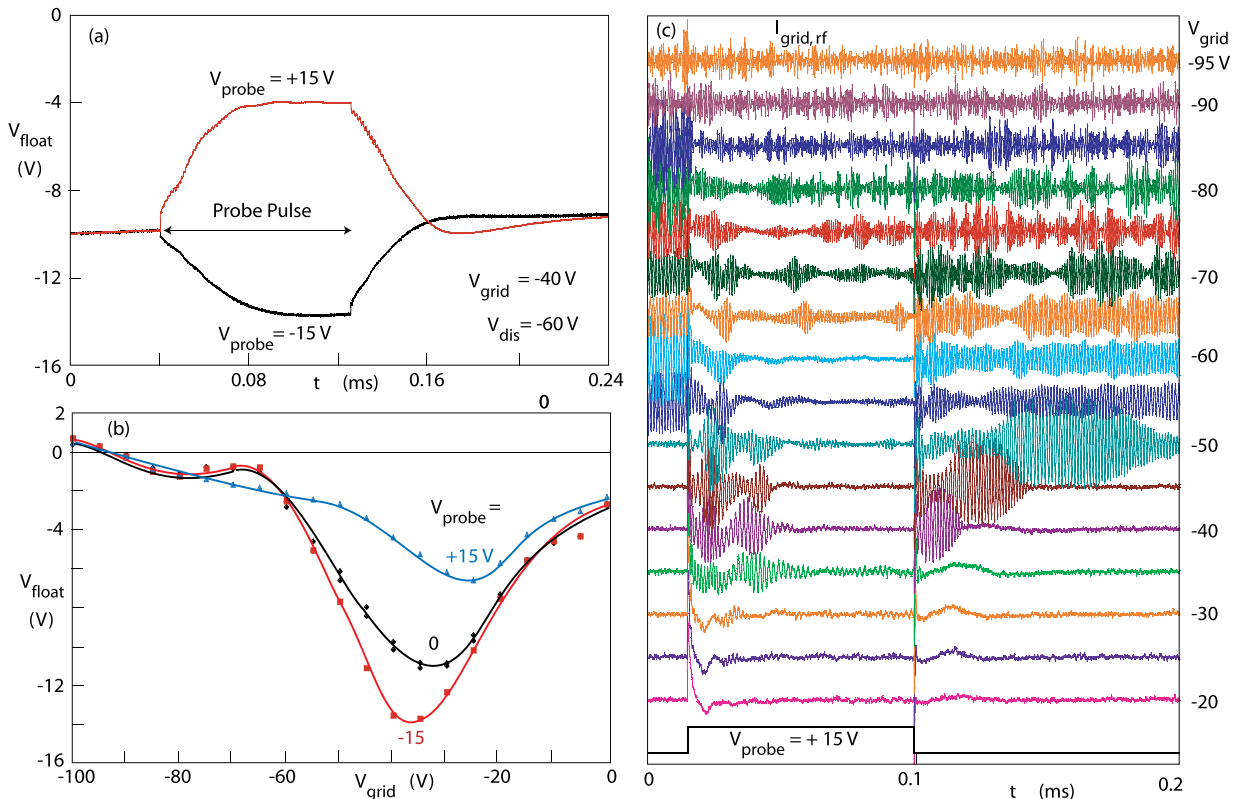


FIG. 6. Bubble modification by a long pulse to an electrode in the center of the 8 cm diam sphere. (a) Floating potential of a probe near the inner sheath, $r_{probe} \simeq 4$ cm. The floating potential is strongly shifted by both positive and negative pulses. The slow rise and decay times are governed by the ions. (b) Floating potential vs grid voltage during the pulse showing that the perturbation is strongest when the potential is near its minimum. (c) Modification of the sheath instability by the positive pulse. A negative pulse produces negligible changes in the grid current oscillations since ion collection is negligible compared to the ion inflow (not shown). The instability is strongest when the electron supply is restricted, which occurs during the positive pulse. For $|V_{grid}| > V_{dis} = 60$ V, the pulse has no effects since the center of the bubble is empty while virtual anode oscillations exist near the grid.

than prior to the pulse. Lowering the electron density must also reduce the ion density which accounts for the slow potential adjustment. After the end of the applied pulse the frequency increases slowly, indicating that the ion density must have been depressed during the pulse. For $|V_{grid}| > V_{dis}$, the potential change is negligible but the probe-induced electron depletion promotes the early formation of virtual anode oscillations.

D. Triggering the instability

Pulsing the probe positively creates perturbations in potential and density inside the bubble. When the trigger pulse is made as short as the instability period, the growth of the sheath instability can be observed. Transient sheath ringing effects are also generated.

Figure 7 shows the response in the grid and probe currents when a positive trigger pulse (+10 V peak, -20 V baseline, 1 μ s length) is applied to a probe in the center of the bubble. The oscillations in the grid current for different dc grid voltages are shown in Fig. 7(a). For $|V_{grid}| < V_{dis} = 60$ V, low-frequency (<100 kHz) oscillations are excited. These are transient phenomena which die out after a few cycles. Their frequency is lowest where the floating potential assumes a minimum or the injected ions have the largest velocity. The period corresponds approximately to the transit time of fast ions through the sphere. Thus, the trigger pulse causes a ballistic ion signal to travel from one side

of the grid to the other, which triggers the next pulse and the process repeats but decays.

For $|V_{grid}| > V_{dis} = 60$ V, higher frequency (700 kHz) oscillations are excited. These also exist at a lower level prior to the trigger pulse and continue after the pulse without damping. They are the sheath plasma instability near the ion plasma frequency. Their frequency and amplitude also vary with V_{grid} which is best seen on an expanded time scale shown in Fig. 7(b). The instability has a large amplitude and low frequency at $V_{grid} \approx 65$ V. For $|V_{grid}| \gg V_{dis}$, the bubble is empty and the probe has no effect on the virtual anode oscillations near the grid. The frequency dependence of the triggered instability on V_{grid} mirrors that of the steady-state instability [Figs. 3(a) and 5(f)].

The oscillations in the probe current have the same character as those in the grid current. The contour plot of Fig. 7(c) shows low-frequency transients, the sheath instability, and virtual anode oscillations of the inner bubble sheath. Since the probe is near the grid, the virtual anode oscillations are detected, although weaker than those in $I_{grid,rf}$ showing that the positive space charge layer extends a few mm beyond the grid. No virtual anode oscillations are observed in the center of the bubble [Fig. 5(b)].

By comparing probe and grid signals, a timing difference is observed. The low-frequency perturbation is first seen on the probe, followed by a delayed one on the grid. Thus, the perturbation travels toward the grid and must have originated from the center or opposite side of the sphere.

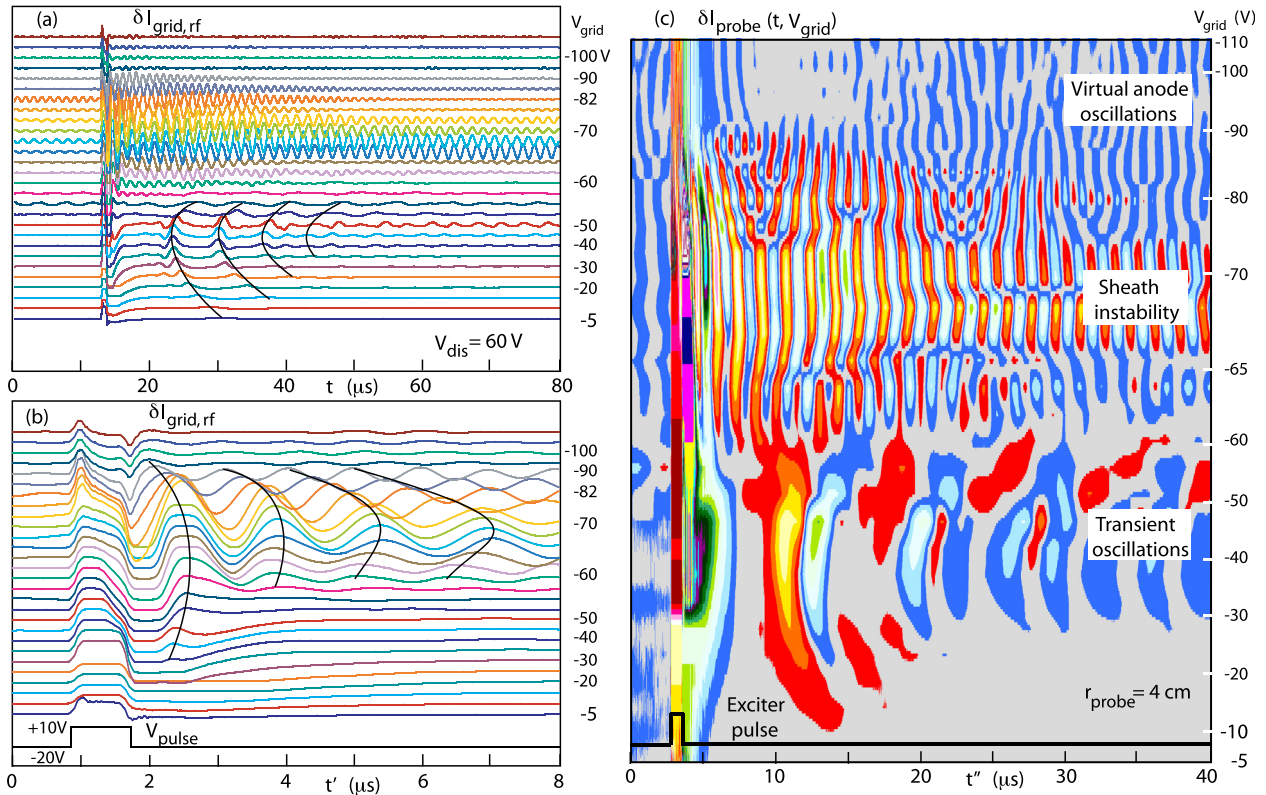


FIG. 7. Triggering sheath oscillations with a short pulse applied to an electrode in the center of the sphere. (a) Oscillations in the grid current vs time for different grid voltages. For $|V_{grid}| < V_{dis}$, low frequency transient oscillations are excited which decay in time. For $|V_{grid}| > V_{dis}$, the high frequency sheath instability is excited. (b) Evolution of the high frequency instability on an expanded time scale t' . The frequency increases with $|V_{grid}|$ and becomes a virtual anode oscillation when electrons cannot enter into the bubble. (c) Contour plot of the oscillations in the probe ion current near the inner sheath. Three different modes of oscillations can be distinguished.

Spatially resolved probe measurements have revealed the properties of the ballistic ion signal. Figure 8(a) shows the perturbed ion current recorded at different radial positions. Except for the first transient response, there is no phase shift or time lag with radial position. Thus, the potential oscillates uniformly throughout the bubble. However, the distortion in the first transient response indicates a traveling signal which has been extracted by subtracting the first trace ($r_{probe} = 4$ cm) from all others. The difference signal, shown in Fig. 8(b) clearly shows a traveling maximum and minimum. The time-of-flight diagram in Fig. 8(c) yields the propagation speed and direction. The perturbation propagates at a radial speed $v_r = 7 - 9 \times 10^5$ cm/s from the sheath into the bubble center *toward* the exciter probe. If it was an ion acoustic wave, it should have propagated *away* from the exciter. Thus, the sheath has been perturbed by the probe-induced potential rise which velocity-modulated the injected ions. The observed velocity would match that of streaming ions with energies in the range 9–18 eV which is

the approximate potential difference between inside and ambient plasma potentials.

The major pulses in Fig. 8(a) repeat in intervals of $\Delta t \simeq 8 \mu\text{s}$ which is close to the travel time of 18 eV ions through the 8 cm diam bubble. Thus, the perturbations travel from one side of the bubble to the other and repeatedly excite new but smaller perturbations that ride inward with the injected ions.

Next, we demonstrate how the higher frequency sheath oscillations start after applying a trigger pulse. For this purpose, the dc grid bias is increased to the discharge voltage so as to restrict the electron inflow. The positive pulse, shown in Fig. 9(a), is applied to the cold emissive probe in the center of the bubble. Figure 9(b) shows the simultaneously measured ac currents from the grid and the negatively (−90 V) biased Langmuir probe located approximately 5 mm from the grid inside the bubble. Probe and grid rf currents are predominantly capacitively coupled signals which are proportional to the plasma potential rather than ion conduction currents.

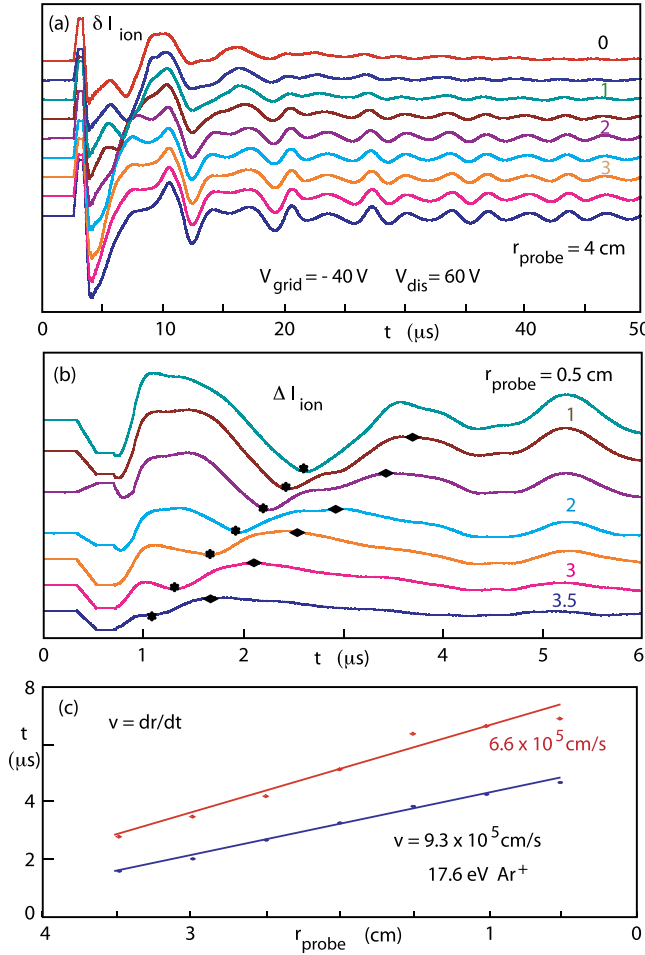


FIG. 8. Radial dependence of oscillations triggered by a short positive pulse to a fixed probe in the center of the bubble. (a) Oscillations in the movable probe current ($V_{probe} = -100$ V) for different radial positions in the 8 cm diam sphere. The lack of phase shift indicates plasma potential variations throughout the bubble. (b) At early times transient ion perturbations, embedded in (a), propagate from the sheath into the bubble. (c) Time-of-flight of the perturbations yield their radial velocities which are well above the sound speed and close to the ion energy acquired by the potential difference between the ambient and bubble plasmas.

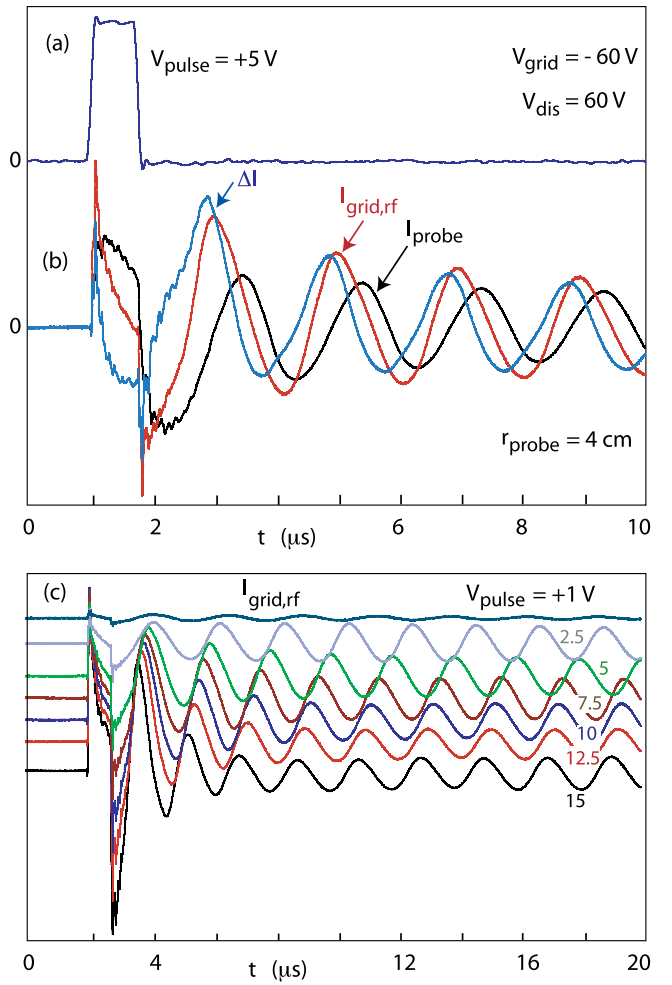


FIG. 9. Triggering the sheath oscillations with a positive pulse (a) applied to a probe in the center of the bubble. (b) Response of grid and probe currents which are proportional to potentials on two sides of the sheath. The difference signal is a measure for the sheath electric field. Ion motion and sheath electric field oppose. (c) Frequency of the sheath instability increases with pulse amplitude due to the change in electron density in the sheath.

When a positive pulse is applied to the center electrode, electrons are drawn from the bubble plasma. They are not supplied from the ambient plasma which shows no potential perturbations. Furthermore, the probe traces are similar in an afterglow plasma where no electrons can enter the bubble. The collected electrons are displaced from the sheath into the plasma which increases the positive charge density in the sheath, hence electric field and plasma potential inside the bubble. The conduction current to the exciter probe closes via the displacement current to the grid and ground. The potential changes occur on the electron time scale. The ions respond on a slower time scale. The increased electric field accelerates the bubble ions toward the grid and decelerates the injected ions. The applied pulse is switched off at about one ion transit time through the sheath. At this time, the observed ac potential is negative, i.e., the space charge density in the sheath ($n_i - n_e$)e is reduced due to the returning electrons and ion outflow.

A negative potential perturbation produces a radially inward pointing ac electric field which decelerates the bubble ions and repels electrons such that after an ion inertial time through the sheath the space charge in the sheath, hence potential, increases. Figure 9(a) shows that the ac grid signal leads with respect to the probe signal. The difference signal $\Delta I = I_{grid} - I_{probe}$ is proportional to the potential drop across the sheath. During the potential rise, the electric field points radially inward, during the potential drop it is negative or points outward. However, when the potential rises the ions still move into the sheath, i.e., opposite to the electric field. The oscillation arises from particle inertia and field restoring force.

In its simplest form, the sheath dynamics can be described by a slab of ions displaced from a neutral plasma by a distance x . The surface charge density $\sigma = en_i x$ produces an electric field $E = en_i x / \epsilon_0$ which leads to a simple equation of motion, $m_i d^2x/dt^2 = e^2 n_i x / \epsilon_0$ describing an oscillation at the ion plasma frequency $\omega_{pi} = [e^2 n_i / m_i \epsilon_0]^{1/2}$. However, the sheath on a highly transparent grid contains counter streaming ions and electrons. The net charge density becomes $(n_i - n_e)e$ which lowers the oscillation frequency below the ion plasma frequency. One example where this becomes evident is shown in Fig. 9(c). When the pulse amplitude is raised, more electrons are extracted from the bubble which increases the charge density and raises the frequency. No frequency shift with amplitude is observed for negative pulses.

The role of the electrons on the instability frequency is now evident. The electron density is controlled by the grid dc bias. As V_{grid} becomes more negative, the floating/plasma potential assumes a minimum. The injected electrons are decelerated and by flux conservation build up a high density leading to a low frequency. For increasingly negative grid voltages, the potential increases and the electron density declines, which results in an increase in frequency. Further examples of frequency drop with electron injection by emissive probe will be shown in a companion paper.¹⁹

IV. CONCLUSION

The time-dependence for creating a bubble with its instabilities has been investigated by pulsing relevant

plasma parameters. Comparing discharge and afterglow plasmas, the trapping of electrons in a bubble has been demonstrated. The instability persists throughout the afterglow without a supply of ambient electrons. From the frequency decay of the sheath instability, the density decay inside the bubble has been found to be comparable to the ambient density decay.

Pulsing the grid voltage yields the time rate for filling and emptying the plasma bubble. The rate is controlled by the lowest particle flux, which is the electron flux for highly negative grid voltages. It is not possible to rapidly modulate the density of a bubble with fast grid voltage pulses.

Inserting biased probes into the bubble upsets the flux balance and thereby perturbs the plasma potential and modifies the sheath oscillations. The I-V characteristics of a Langmuir probe develop a negative differential resistance near the plasma potential and is not useful for diagnostic purposes. A positively biased probe can destroy the electron trapping in an afterglow plasma and raise the instability frequency to that of virtual anode oscillations. Pulsing the probe voltage shows that the time scale for potential relaxation increases as the electron inflow is reduced by biasing the grid more negatively.

Using a short trigger pulse transient sheath oscillations have been excited. Low frequency ringing has been observed for $|V_{grid}| \leq V_{dis}$ and explained by transit time effects of ballistic ions through the bubble. For $|V_{grid}| \geq V_{dis}$, the sheath instability has been triggered. By comparing the potential oscillations across the sheath, the mechanism of the instability has been clarified. Due to the limited electron flux ($I_{el} < I_{ion}$), the ions determine the sheath potential perturbations. Due to inertia, the ions lag by 180° behind the space charge electric field which results in the sheath oscillation. Electrons in the sheath reduce the net space charge which lowers the frequency below the ion plasma frequency. The frequency dependence on V_{grid} is explained by the effects of electrons in the sheath.

ACKNOWLEDGMENTS

The authors gratefully acknowledge support from NSF/DOE Grant 20101721 and AFRL Contract FA8721-11-C-0009.

- ¹R. L. Stenzel, *Phys. Fluids B* **1**, 2273 (1989).
- ²Y. P. Bliokh, J. Feltsteiner, and Y. Z. Slutsker, *J. Appl. Phys.* **111**, 013302 (2012).
- ³P. J. Barrett and R. G. Greaves, *Phys. Fluids B* **1**, 1776 (1989).
- ⁴J. Chutia, S. Sato, H. Kubo, and Y. Nakamura, *J. Plasma Phys.* **46**, 463 (1991).
- ⁵G. Popa and R. Schrittweiser, *Phys. Plasmas* **1**, 32 (1994).
- ⁶A. Sarma, H. Bailung, and J. Chutia, *Phys. Plasmas* **4**, 61 (1997).
- ⁷H. Klostermann, A. Rohde, and A. Piel, *Phys. Plasmas* **4**, 2406 (1997).
- ⁸T. J. T. Kwan, *Phys. Fluids* **27**, 228 (1984).
- ⁹A. Rohde, A. Piel, and H. Klostermann, *Phys. Plasmas* **4**, 3933 (1997).
- ¹⁰R. L. Stenzel, J. M. Urrutia, C. Ionita, and R. Schrittweiser, *Phys. Plasmas* **17**, 062109 (2010).
- ¹¹R. L. Stenzel, J. Gruenwald, C. Ionita, and R. Schrittweiser, *Phys. Plasmas* **18**, 062113 (2011).
- ¹²M. Sanduloviciu and E. Lozneanu, *Plasma Phys. Controlled Fusion* **28**, 585 (1986).

- ¹³B. Song, N. D.'Angelo, and R. L. Merlino, *J. Phys. D: Appl. Phys.* **24**, 1789 (1991).
- ¹⁴L. Conde, C. F. Fontn, and J. Lambs, *Phys. Plasmas* **13**, 113504 (2006).
- ¹⁵D. G. Dimitriu, M. Afliori, L. Ivan, C. Ionita, and R. Schrittweis, *Plasma Phys. Controlled Fusion* **49**, 237 (2007).
- ¹⁶S. D. Baalrud, B. Longmier, and N. Hershkowitz, *Plasma Sources Sci. Technol.* **18**, 035002 (2009).
- ¹⁷R. L. Stenzel, J. Gruenwald, C. Ionita, and R. Schrittweis, *Plasma Sources Sci. Technol.* **21**, 015012 (2012).
- ¹⁸R. L. Stenzel and J. M. Urrutia, *Phys. Plasmas* **19**, 082105 (2012).
- ¹⁹R. L. Stenzel and J. M. Urrutia, *Phys. Plasmas* **19**, 082107 (2012).
- ²⁰R. L. Stenzel, J. Gruenwald, B. Fonda, C. Ionita, and R. Schrittweis, *Phys. Plasmas* **18**, 012104 (2011).
- ²¹R. L. Stenzel and J. M. Urrutia, *Phys. Plasmas* **4**, 26 (1997).